A personalized network framework reveals predictive axis of anti-TNF

2 response across diseases

- 3 Shiran Gerassy-Vainberg^{1,2}, Elina Starosvetsky^{#1}, Renaud Gaujoux^{#1,4}, Alexandra Blatt*², Naama
- 4 Maimon^{1,2}, Yuri Gorelik², Sigal Pressman², Ayelet Alpert¹, Haggai Bar-Yoseph^{1,2}, Tania Dubovik¹, Benny
- 5 Perets¹, Adir Katz⁴, Neta Milman¹, Yehuda Chowers^{*1,2,3}, Shai S. Shen-Orr^{*1}
- 6 on behalf of the Israeli IBD research Network (IIRN)
- 7 #, * Contributed equally to the study

Author affiliations

1

8

14

19 20

- 10 1. Faculty of Medicine, Technion-Israel Institute of Technology, Haifa, Israel
- 2. Department of Gastroenterology, Rambam Health Care Campus, Haifa, Israel
- 12 3. Clinical Research Institute, Rambam Health Care Campus, Haifa, Israel
- 4. CytoReason, Tel Aviv 67012, Israel

15 Corresponding author contact information:

- Shai Shen-Orr, Faculty of Medicine, Technion-Israel Institute of Technology, Haifa 32000, Israel;
- 17 shenorr@technion.ac.il and Yehuda Chowers, Department of Gastroenterology, Rambam Health Care
- 18 Campus, Haifa, Israel; <u>y chowers@rambam.health.gov.il</u>.

Abstract

21

31

35

36 37

38

39

40

41

42

43 44

45

61

22 Personalized treatment of complex diseases is an unmet medical need pushing towards drug biomarker 23 identification of one drug-disease combination at a time. Here, we used a novel computational approach 24 for modeling cell-centered individual-level network dynamics from high-dimensional blood data to predict 25 infliximab response and uncover individual variation of non-response. We identified and validated that 26 the RAC1-PAK1 axis is predictive of infliximab response in inflammatory bowel disease. Intermediate 27 monocytes, which closely correlated with inflammation state, play a key role in the RAC1-PAK1 responses, 28 supporting their modulation as a therapeutic target. This axis also predicts response in Rheumatoid

29 arthritis, validated in three public cohorts. Our findings support pan-disease drug response diagnostics

30 from blood, implicating common mechanisms of drug response or failure across diseases.

Keywords

- 32 Precision medicine, Individual-level network analysis, Drug response, Anti-TNF antibodies, Infliximab,
- Immune-mediated diseases, Inflammatory bowel disease, Rheumatoid arthritis, Pan-disease drug 33
- 34 response diagnostics.

Introduction

- Biologic therapies are widely used in a broad range of therapeutic areas including immune-mediated diseases, oncology and hematology and have demonstrated effectiveness by improving disease clinical course, morbidity and patient quality of life. However, a sizable fraction of patients does not respond to therapy and is exposed to the consequences of uncontrolled disease activity, unwanted side effects and increasing care costs. Therefore, the development of biomarkers for response prediction is an unmet medical need, necessary for achieving a favorable therapeutic index, cost/benefit ratio and overall improved patient care. Although biologics' targets are highly specific (e.g. PD1, TNFα) and target particular molecular processes across diseases (e.g. CD8 T-cell exhaustion, or TNF induced inflammation), presence of these processes in an individual patient is necessary but not sufficient to predict response, implying a
- 46 One of the most frequently used biologic drug classes are anti-TNF α antibodies, with sales of over \$US 25 47 billion per year³. Anti-TNF agents are thought to exert their effects through several mechanisms, including TNFα neutralization, induction of cell and complement cytotoxicity through the FC drug fragment and 48
- 49 cytokine suppression via reverse signaling or apoptosis⁴. Similar to other drugs and across target diseases
- 50 including inflammatory bowel disease (IBD) and rheumatoid arthritis (RA), a sizable proportion of 20-40%
- 51 of the treated patients, will primarily not-respond to treatment^{5,6}.

more complex therapeutic mechanism which may be disease specific^{1,2}.

52 Previous studies used systematic screening of in-house and meta-analysis data for the identification of 53 biomarkers associated with anti-TNF α treatment failure. Different markers were identified in different 54 disease contexts⁷. Among these, in IBD, Oncostatin M (OSM) was identified as a potent mucosal biomarker8. This gene correlated closely with Triggering Receptor Expressed On Myeloid Cells 1 (TREM1), 55 a biomarker found by us, which was predictive of response in biopsy and importantly also in blood, albeit 56 57 in an inverted ratio⁹. In RA, myeloid related sICAM1 and CXCL13, and type I IFN activity were associated 58 with anti-TNF response¹⁰. The identification of these markers suggests that biomarkers of pretreatment 59 immune status may be useful for patient screening. However, little is known regarding molecular 60 dynamics of anti-TNF response and resistance, and whether drug biomarkers are disease dependent, or

The availability of high-resolution molecular data provides opportunities for achieving improved modeling of the complex therapeutic landscape using systems biology and network-based approaches. Yet, most of the statistical methods used are based on population averages, which do not suffice to fully investigate these complex diseases. Although several personalized approaches were recently suggested for exploring sample-level network information^{11,12}, these studies were not cell-centered, and did not decouple cell frequency and cell regulatory program changes. Network structure was used to identify individual alterations in cross-feature relationships between groups, however, these were validated only in the unicellular level. The same is true for the identification of individual-level time series analysis.

Here we employed a longitudinal cell-centered systems analysis, combining high-dimensional data of whole blood from anti-TNF responding and non-responding IBD patients at baseline and following two and fourteen weeks post first treatment. We focused on immune responses in blood, because although presenting an analytical challenge due to high background noise, blood-biomarkers have a clear advantage of accessibility and cost-effectiveness for therapeutic purposes. To understand individual variation in drug resistance, we devised a single sample-based network approach, termed 'Disruption Networks', which provides patient specific hypotheses for lack of response with respect to a global response network. Using this approach, we demonstrate that monocytic RAC1-PAK1 axis expression, which is a final common pathway of multiple immune-receptor signaling cascades, is predictive of anti-TNF response in IBD as well as for the same treatment in RA, providing validation for the signature's predictivity and supporting common baseline elements that contribute to response across infliximab (IFX) treated immune mediated diseases.

Results

Treatment response is associated with forward movement along an immune health axis, whereas non-responders regress.

To understand the cellular and molecular changes associated with IFX response and non-response, we performed longitudinal deep immunophenotyping of peripheral blood in Crohn's disease (CD) patients who received first-time therapy with IFX during standard clinical care (Fig. 1a, left, hereon IFX cohort). Patients were profiled a total of three times: pre-treatment (day 0), week 2 (W2) and week 14 (W14) post-treatment initiation. At W14, 15 patients showed clinical response whereas 9 were classified as non-responders at the study end (Supp. Table 1 for clinical demographics; see Methods for response classification).

Complementary to this, to define an individual-specific unbiased expectation of peripheral blood immune dynamics during disease course, we used a public gene expression dataset of whole blood samples from healthy individuals and 75 IBD patients in varying disease states treated with standard of care drugs (Fig. 1a; see Methods). We constructed an external data-driven reference IBD axis (Fig. 1b, left), which describes in a dimensionality reduced Principal Component Analysis (PCA) space the molecular transition from active- through inactive disease to healthy- state, based on differentially expressed genes (hereon 'Health axis', see Methods). Next, we projected the position of our in-house IFX cohort on the PCA (Fig. 1b, right) and calculated the distance each patient traversed on the axis along the course of time, providing continuous molecular information to characterize a patient's immune state shift (Fig. 1c). Analyzing the distance between paired sample time-points, we observed that responders progressed on the health axis (*i.e.*, a positive shift on the axis towards the centroid of healthy reference samples), while non-responders regressed on it (Figure 1c, *P*<0.05, one-sided permutation test). Breaking up these

dynamics by time point, we observed that responders exhibited increased progress along the health axis following first drug treatment, and reduced progress in the following period (Figure 1c). The negative correlation between progress along the axis between baseline-W2 and progress in the following segment W2-W14 suggests that patients progressing to 'response' early, slow down during the following visit whereas those showing a slow progress initially, progress more thereafter (Fig. 1d). Importantly our results suggest that clinical non-responders are immunologically affected by treatment as well, with an overall opposite direction from responders' progress. Collectively, our health axis, captures blood molecular changes which are clinically relevant for treatment response.

Early IFX response reduces expression of innate immune pathways attributed mainly to monocytes

114 function.

105

106

107

108 109

110

111

112

113

115

116

- To identify changes following treatment in each response group, we characterized major immune cell compositional changes in 16 canonical immune populations (Fig. 2, Supp. Table 2-3 for CyTOF panel and
- 117 Citrus clusters annotation). Then, to compare how peripheral blood state differs as a function of treatment
- 118 response, we computed a PCA on the fold change of patients' cell phenotyping profiles (Fig. 2a, left). We
- 119 observed significant difference in cell abundance changes between responders and non-responders for
- 120 W2 and W14 changes relative to baseline (P=0.005, NPMANOVA).
- 121 Multiple cell subset changes in responders were already apparent at W2 including reduced abundance of 122 monocytes, granulocytes, Tregs, naïve CD4+ T cells, CD4+ central memory T cells and increased abundance 123 of CD4+ and CD8+ effector memory T cells and B cells (FDR≤0.15, Paired Wilcoxon test; Supp. Fig. 1a). Based on the PCA loadings we deduced that monocytes and Tregs were the prime drivers of changes 124 125 following treatment (Supp. Fig. 1b), evidence for which was also supported by the univariate comparison
- 126 showing that monocytes were significantly reduced in responders throughout both W2 and W14, whereas
- 127 in non-responders monocyte frequency was unchanged in W2 and elevated at W14 (P=0.0015 and
- 128 P=0.048 in responders, as opposed to P=0.64 and P=0.016 in non-responders at W2 and W14 respectively,
- 129 Paired Wilcoxon test). Moreover, monocyte frequency was also correlated with changes in CRP
- 130 (Spearman's r = 0.4, P = 0.01), suggesting their relevance to treatment response (Fig. 2a center, right and
- 131 Supp. Fig. 1c for correlation of CRP with other cell-types). Taken together, our results demonstrate
- 132 significant differential cell composition following IFX treatment as a function of response, with monocytes
- 133 likely playing a major role.

134 Given the observed cell composition alterations, we performed a cell-centered analysis to identify changes in transcriptional programs following treatment in each response group, by adjusting the gene 135 expression for variation in major cell-type proportions. This procedure places focus on detection of 136 differences between conditions of the gene regulatory programs the cells are undergoing rather than 137 those differences detected due to cell compositional differences, and has been shown to unmask 138 139 additional signal (i.e. false-negative of direct bulk analysis) while decreasing false-positives (Fig. 2b, see Methods)9. In this analysis, we identified 1400 (5.99%) and 589 (2.52%) differential features in responders 140 141 (FDR<0.15, permutation test; Supp. Tables 7) at W2 and W14 compared to baseline respectively, 142 suggesting enhanced response at W2 followed by reduced dynamics in W14. Compared to responders, non-responders showed attenuated dynamics in the parallel treatment periods, with only 542 (2.32%, 143 144 Supp. Table 7) differential features at W2 compared to baseline, and no significantly detected dynamics 145 at W14. To ensure the differences in dynamics between the two response groups were not due to sample size, we subsampled responders to match the non-responder group size and observed that responding 146 147 patients exhibit more dynamic changes compared to non-responders (Supp. Fig. 2). Furthermore,

comparing the two response groups, we observed only a minor overlap in the post treatment dynamic

features (23 features, 1.2% at W2). In line with the 'health axis', these results suggest that there are

increased early dynamics in responders compared to non-responders and that responders and non-

responders presented different alterations following treatment.

149

151

152

153

154

155

156

157

158159

160

161162

163164

165

166

167

168 169

170

171

172173

174

175

176

177

178

179

180

181

182

183

184

185 186

187

188 189

190

191192

measurements (Fig. 2c).

To understand the relationship during IFX response between gene regulatory programs in a biological context, we constructed a cell-centered co-expression network, which was expanded by known interacting genes, followed by functional enrichment analysis (see Methods, Supp. Tables 8 for network edges and Supp. Fig. 3b for functional enriched pathways respectively). Interestingly, despite this being a blood-based network, we noted genes which were previously associated with anti-TNF response in IBD biopsies such as TREM1 and OSM^{8,9}, suggesting that relevant signals originally detected in tissue, are also reflected in blood. We identified potential mediating pathways, i.e. pathways possessing higher connectivity to other nodes in the response network, using degree and betweenness centrality

We observed that most central pathways associated with the W2 early response were related to the innate immune system (Supp. Fig. 3b). At the pathway level, consistent with the 'health axis' and feature level analysis, we found augmented response at W2, which was attenuated in the following period (151 vs. 88 enriched dynamic pathways in responders at W2 and W14 respectively; Supp. Fig. 3a-b). As expected, among the innate related altered functions, we observed pathways related to downregulation of NF-kB and TNF signaling via NF-kB (Fig. 2c, FDR<0.005 for W2 vs. baseline pathway score comparison, by Wilcoxon test; FDR<0.01 for enrichment in network by GSEA). Pathways with high network centrality included downregulation of FC receptor signaling and phagocytosis, cytoskeleton organization, Toll-like receptors (TLRs) and vascular endothelial growth factor (VEGF) signaling responses (Fig. 2c; top 25th percentile for both degree and betweenness; FDR<0.005 for W2 vs. baseline, by Wilcoxon test; FDR<0.1 for enrichment by GSEA). These pathways also correlated with CRP measured in the clinical setting (Spearman's r FDR<0.05 and Supp. Fig. 3d). Of note, FCYR is known to be regulated by TNF α^{13} and mediates a number of responses, including the phagocytosis of IgG-coated particles, accompanied by cytoskeleton rearrangements and phagosome formation, central pathways that were downregulated in responders (Fig. 2c and Supp. Fig. 3b, FDR<0.001 for W2 vs. baseline, by Wilcoxon test; FDR<0.15 for enrichment by GSEA). We also observed the downregulation of reactive oxygen species (ROS) pathway, which is crucial for the digestion of engulfed materials in phagosomes (FDR<0.001 for W2 vs. baseline, by Wilcoxon test; FDR<0.05 for enrichment by GSEA). This pathway was also correlated with CRP (Spearman's r 0.43, FDR<0.005, Supp. Fig. 2b and Supp. Fig. 2d). To identify the most likely cell expressing these pathways, we regressed the unadjusted fold change gene expression on major blood immune cell abundance changes (see Methods). We observed that monocytes and granulocytes were the major contributors associated with the dynamic pathways (Supp. Fig. 3c). This further supports the considerable contribution of monocytes to treatment response, on top of their significant frequency alteration and their frequency correlation with CRP.

'Disruption Networks' as a framework to understand individual variation in non-responders' dynamics.

Whether non-responders' transcriptional profile reflects fundamental routes of IFX resistance, is essential for tailoring treatment. To elucidate molecular mechanisms of individual-specific pathways of treatment non-response, we devised a systematic framework we term 'Disruption Networks'. The underlying principle of this method is the study of relations between features across a population of individuals (i.e., a population level reference network), and then infer of how these relations differ (i.e., are disrupted) at the single sample level; providing understanding of how each individual's molecular network behaves in a specific condition.

To identify how non-responding individuals differ with respect to the IFX response dynamics, we iteratively added a single non-responding patient to the response reference network we had studied and calculated the disruption in the correlation structure in each edge for that patient (hereon 'dropout'). This procedure was performed separately for each non-responder. We considered only negative dropouts, that is, events in which the relation (i.e., correlation) between two features was weakened once the non-responder data was spiked into the responders' group, indicating deviance from treatment response (Fig. 3a right, for an example). To evaluate non-responders' dropout significance, we generated empirical null distribution of dropouts ('normal response' dropouts) by iterative addition of each responder's sample to the other responders' samples. We calculated P-values as a left-tail percentile, within the null distribution of the normal dropouts, which were further corrected for multiple testing (Fig. 3a; see Methods). By applying the 'Disruption Networks' framework, we considerably expanded the detected differential signal between response groups as compared to standard differential analysis (one feature by Wilcoxon test (FDR<0.1) vs. 180 features by mean drop intensity, including the single feature identified by Wilcoxon test (FDR<0.1 for dropout significance and 10th top percentile of mean drop intensity); Fig. 3b and Supp. Fig. 4a-b for mean drop intensity, disrupted edge ratio parameters and the agreement of both respectively).

To understand disruption in the functional context, we aggregated the dropouts to calculate a pathwaylevel personalized disruption (Fig. 3c; see Methods). We found that the major disrupted dynamics at W2 was related to the cytoskeleton/fiber organization and VEGFR signaling which were central functions during normal treatment dynamics. Interestingly, nodes related to these disrupted pathways exhibited high centrality (P<9.999e-05 and P=0.034 for degree and betweenness correspondingly by permutation test; Fig. 3d). On the meta-pathway level, monocytes were the most central cell-type associated with the disrupted pathways (Fig. 3e, left, top 5th percentile for degree and betweenness centrality). The disrupted meta-pathway included the core genes consisting of the HCK-RAC1-PAK1 signaling cascade, which presented high combined degree and betweenness centrality (P=0.017, n=1000 random triple node subsampling). This core perturbed axis is a final common pathway involving signaling through several proximal immune-receptors by a range of inflammatory ligands including chemokines, growth factors such as VEGFR, and FC receptor ligands which induce FC-mediated phagocytosis involving coordinated process of cytoskeleton rearrangement¹⁴. Indeed, these pathways were functionally enriched in the disrupted meta-pathway (q-value<0.05, hypergeometric test; Fig. 3e, right). The latter are also linked to ROS and NADPH oxidase activation through the regulation of RAC1¹⁵.Of note, suppression of RAC1-PAK1 signaling, predominately in innate immune cells was shown to mediate remission in CD¹⁶. Taken together, these observations showcase the power of 'Disruption Networks' to identify masked, individual level, signal and suggest that the RAC1-PAK1 signaling cascade, is significantly disrupted in non-responders, during treatment.

RAC1-PAK1 signaling is elevated in responders' peripheral monocytes pre-treatment.

We next asked whether cellular programs found to be disrupted during treatment dynamics can be identified pre-treatment, since direct differential analysis in the feature expression space did not yield significant signal. Looking at the feature level, we found that most of the pre-treatment differentially expressed genes were increased in responders, including genes involved in the RAC1-PAK1 axis (FDR<0.1, Wilcoxon test, Supp. Fig. 5a). On the pathway level we observed that the fiber organization pathway, presented pre-treatment disparity between the two response groups (FDR<0.1, NPMANOVA) and correlated with clinical CRP (Spearman's r =0.4, P=0.06), in addition to its high centrality in the response network (Fig. 4a, left). The relative pathway score of the cytoskeleton-organization pathway was higher in responders pre-treatment compared to non-responders (P<0.0006, one-tailed Wilcoxon test), and was downregulated following efficient treatment (P<0.001 and P<0.05 for W2 and W14 compared to baseline,

one-tailed Wilcoxon test). This was in contrast to non-responders which showed insignificant dynamics at

W2 and even an opposite trend in W14 (P=0.52 and P=0.041 for W2 and W14 compared to baseline, one-

tailed Wilcoxon test) (Fig. 4b).

The fiber organization pathway associated with treatment dynamics and response already at pretreatment state, represents distinctive differences in cellular transcriptional states between response groups, rather than differences reflecting cellular composition alterations, as our analyses accounted for cell proportions. Therefore, we next aimed to dissect the cellular origin of the fiber organization related core genes. First, we tested the correlation between the canonical cellular frequencies as obtained by CyTOF, and the bulk unadjusted expression of the fiber organization genes (Supp. Fig. 5b). We observed that the majority of the genes in the target pathway were positively associated with monocytes abundance. To further validate the cellular origin and the fiber organization related transcriptional cell state in the two response groups, we performed single-cell RNA sequencing (scRNA-seq) using peripheral blood mononuclear cells (PBMCs) from pre-treatment samples of representative responder and non-responder patients (Fig. 4c, left; see Methods). Assessment of the fiber organization related expression in the cellular level, confirmed that monocytes were highly associated with the distinctive pathway expression (*P*<2.2e-16, for expression in monocytes compared to the other cell types, Wilcoxon test, Fig. 4c, right and Supp. Fig. 6a).

To understand the molecular events associated with the fiber organization pathway in the relevant cell and subset specific context, we expanded the fiber organization differential genes through intersection of knowledge- and data-driven based networks (see Methods). Then, we assessed the pathway related expression in monocyte subsets, which were previously shown to exhibit distinct phenotypes and functions in health, and immune-mediated disease states¹⁷. The results indicated that intermediate monocytes contributed most to the fiber organization distinctive expression between the response groups, pre-treatment (|FC|=2.13, P<2.2e-16 in intermediate monocytes vs. |FC|=1.3, P<2.2e-16 and |FC|=1.1, P<0.05 in classical and non-classical monocytes respectively by Wilcoxon test, Fig. 4d). Interestingly, we detected significantly increased membrane TNF (mTNF) on intermediate monocytes compared to the other subsets (P<5e-07, one-tailed Wilcoxon test, Fig. 4e), suggesting these cells serve as drug targets, thereby explaining their tight linkage to drug response.

Pre-treatment RAC1-PAK1 axis is predictive for IFX response across immune mediated diseases.

We next tested whether the pre-treatment fiber organization pathway could predict treatment response (see Methods). We observed that the pathway score of a set of 6 core genes (RAC1, PAK1, LYN, ICAM1, IL1B and FCGR3A) could discriminate responders from non-responders at a mean AUC of 0.90 (95CI 0.74, 1; P=0.0001 by Permutation test), supporting a common mechanism of non-response to treatment (Fig. 5a). By applying targeted network analysis of the predictive fiber organization pathway in intermediate monocytes, we found that the FCYR signaling and functionally related pathways including phagocytosis and ROS metabolism were highly enriched in the co-expression network effectively differentiating

between response groups at baseline (Supp. Fig. 7).

To further validate our findings, we tested an additional independent validation cohort of 29 CD patients, which were naive to biological treatment and were treated with thiopurines or steroids only as a cotherapy (Supp. Table 9 for clinical demographics). The results indicated that the pre-treatment RAC1-PAK1 axis, was differentially expressed between response groups in the validation cohort (*P*<0.01, Wilcoxon

test) as well, supporting the primary findings and thereby demonstrating that reduced pre-treatment expression of the RAC1-PAK1 axis is associated with non-response (AUC=0.78; Fig. 5b).

To assess whether the predictive RAC1-PAK1 axis is disease dependent or whether it could be generalized across diseases, we tested public datasets of blood samples from RA patients, pre-IFX treatment (GSE20690¹⁸, GSE33377¹⁹, GSE42296²⁰). Gene expression was adjusted to major cell type contributions which was evaluated by deconvolution (see Methods). The results confirmed the increased pre-treatment expression of the axis genes in RA responders, (representative cohort GEO20690, Fig. 5c). Application of fiber organization predictive signature to multiple pre-treatment RA cohorts separated IFX response groups effectively (Meta ROC AUC=0.72, Fig. 5d). These findings expand the predictive value of the RAC1-PAK1 axis to other IFX-treated related diseases such as RA. Taken together, these observations demonstrate that the baseline RAC1-PAK1 axis expression in monocytes differentiates response groups and ultimately impacts response potential across diseases.

Discussion

Despite substantial inter-individual heterogeneity and our growing ability to measure it, commonly used statistical frameworks for analyzing high-dimensional data describe changes happening on average between conditions or groups. This is especially true in the case of networks which form a natural way of describing the possible interactions occurring between measured biological species, yet are population-based, and thus limited in their ability to monitor individual variation from those interactions and the ensuing emergent phenomena these interactions yield. Here we studied the dynamics of IFX response in IBD, in a small cohort, over time. To address this challenge, we devised the 'Disruption Networks' approach, a cell-centered personalized statistical framework which unmasks differences between individuals. The approach enables a systematic dissection of IFX effect response dynamics from blood, considering both cellular composition changes and changes in cellular regulatory programs, allowing us to identify robust functional pathways deviating from normal response in non-responders, and robustly associate these with drug resistance in both IBD and RA.

Although TNF is a pleiotropic cytokine, functioning in both the innate and adaptive immune system²¹, we found that the early response alterations following IFX treatment were mostly related to innate pathways of which monocytes were the major driver. Evidence supporting this has been previously implicated by the decreased frequency of monocytes during treatment in anti-TNF treated IBD²² and RA²³ patients. Furthermore, the anti-proliferative and cell-activation suppressive effect of IFX was shown to depend on FC-expressing monocytes in a mixed lymphocyte reaction²⁴. In addition, the regained long term response following granulocyte/monocyte adsorption treatment following loss of response during IFX treatment further corroborates our findings²⁵. Taken together, these results support the potential for subset specific targeted therapy to augment IFX treatment.

By applying the 'Disruption Networks' framework, we identified RAC1-PAK1 signaling, as a central pathway associated with IFX response. This pathway exhibited disrupted dynamics in non-responders and was predictive of treatment response at baseline. Although abnormal RAC1 signaling was linked to immune-mediated diseases pathogenesis²⁶, its direct relation to anti-TNF response has not been demonstrated. The RAC1-PAK1 axis is a final common pathway shared by several proximal immune receptors, controlling actin cytoskeletal movement, activation of the respiratory burst and phagocytic activity in innate cells. RAC1 was identified as a susceptibility gene for IBD²⁷, and TNF was shown to stimulate RAC1-GTP loading¹⁶, supporting efficacy of antagonizing this effect by anti-TNF. In line with our

findings demonstrating IFX suppressive effect on the RAC1-PAK1 axis during treatment, thiopurines, another effective IBD treatment were also shown to inhibit RAC1 activity²⁸. The superior effect of anti-TNF -thiopurines combination over monotherapy²⁹ suggests that the enhanced therapeutic effect is mediated not only by controlling anti-drug antibody (ADA) levels, but conceivably also by the induction of a mutual additive effect on RAC1 suppression. Interestingly, the TREM adaptor (TYROBP/DAP12), which we previously found to be predictive for anti-TNF response by meta-analysis⁹, was detected in the differential RAC1-PAK1 signature, exhibiting significant correlation with the RAC1-PAK1 axis in monocytes, and is also functionally related through shared signaling³⁰.

The monocytes single-cell based RAC1-PAK1 co-expression network demonstrated pre-treatment differential expression, primarily in intermediate monocytes, related to FcyR dependent phagocytosis and interferon signaling. This is consistent with prior reports showing that FcyR affinity affects anti-TNF therapeutic response^{31–33}. Interestingly, RAC1-PAK1 axis was predictive of IFX responsiveness also in RA, an observation which provides additional validation for the signature predictivity and supports common baseline elements contributing to response across IFX-treated immune-mediated diseases. Similarly to IBD, also in RA, the RAC1-PAK1 upstream activator FcyR was linked to disease susceptibility^{34,35}. The FcyR3A is known as a key receptor for monocytes effector response including antibody-dependent cellular cytotoxicity (ADCC), immune IgG-containing complexes clearance and phagocytosis^{36,37}. These further corroborate the common element of enhanced RAC1-PAK1 signaling through increased expression or affinity for FcyR3A expressed on monocytes that may enhance the efficacy of IFX in IBD and RA. These results extend the relevance of molecular commonalities for disease activity³⁸ and pan-pathology³⁹, also to interconnected pathways of drug responsiveness across diseases.

Whether the RAC1-PAK1 axis and the upstream FcyR are applicable to IFX response in other immune-related diseases or other anti-TNF therapeutic antibodies remains to be determined. While we identified the RAC1-PAK1 axis as predictive for IFX response in naive patients, our results do not yet provide an understanding of how this axis is expressed in non-naive patients. Considering the backwards immune shift in non-responders along the 'health axis' we identified, analysis of non-naive patients should be addressed separately. The 'health axis' further provides a potential explanation for the inferior response rates to subsequent treatments in treatment-experienced compared to naïve patients treated with the same agents⁴⁰. Of note, our real-life cohorts consisted of clinically comparable responding and non-responding groups, in terms of demographics and concurrent therapies, except for lower drug levels in non-responders at W14 in the primary cohort. The disrupted axis was identified at the early W2 response period in which drug levels were comparable and thus response is not expected to be affected by the subsequent difference. In this context, the lower drug levels are likely a consequence rather than a cause of non-response, maybe due to "inflammatory sink" drug consumption, or drug loss through a "leaky gut"^{41,42}.

Blood-based pre-treatment biomarkers are highly important for precision medicine, since when identified across diseases and drugs as performed here, they offer the vision of data-driven choices for physician treatment and personalized care. Our results suggest that the road to this vision may be shorter than anticipated, as at least for immuno-therapies, blood is a relevant tissue for signal detection and drug non-response mechanisms appear to be conserved pan-disease. We note that this pan-disease drug response conserved pattern may not necessarily hold in biopsies from the site of disease, which being different tissues, may present different cells playing a role. Our combined experimental-computational approach, where small time series experiments are combined with an individual-level analytical framework, can be

generalized to other diseases and conditions including mechanisms of drug mode of action, drug non-response, comparison of drug effects and disease courses. These will ultimately allow to make sense of blood and accelerate an era of immune-based precision diagnostics.

Methods

Patients and study design

Primary real-life IBD cohort

A primary real-life cohort consisting of 24 Crohn's disease (CD) patients who received IFX treatment at the gastroenterology department of the Rambam Health Care Campus (RHCC). All patients met the study inclusion criteria as follows: 1) Adequately documented active luminal CD, as phenotyped by a gastroenterologist with expertise in IBD. 2) Documented decision to initiate full IFX induction regimen with 5 mg/kg induction dosing (i.e., at weeks 0, 2, 6). Patients that had past exposure to Infliximab, Adalimumab or Vedolizumab, or patients who had active infection including febrile diseases or intra-abdominal or perianal abscess were excluded. The study was approved by the institutional review board (0052-17-RMB), and patients provided written informed consent. Demographic and clinical characteristics of the patients are shown in Supp. table 1.

Patient samples were obtained at three time points: at baseline, before IFX treatment, and two and fourteen weeks post first treatment and assayed for gene expression microarray data, high-resolution granulocytes and lymphocytes subtype frequencies and functional markers by CyTOF, and a panel of 51 cytokines and chemokines by Luminex. CyTOF panel including Clone, vendor, and conjugation information, and Luminex panel are detailed in Supp. table 2 and 3 respectively.

Patient response classification was defined by decision algorithm, which we used and described previously ⁹. Briefly, patients were classified as responders based on clinical remission, which was defined as cessation of diarrhea and abdominal cramping or, in the cases of patients with fistulas, cessation of fistula drainage and complete closure of all draining fistulas at W14, coupled with a decision of the treating physician to continue IFX therapy at the current dosing and schedule. In patients that were initially clinically defined as partial responders, classification was determined by a decision algorithm that included the following hierarchical rules: 1) steroid dependency at week fourteen; 2) biomarker dynamics (calprotectin and CRP) and 3) response according to clinical state at week 26. Applying the decision algorithm and exclusion criteria, yielded a final study cohort of 15 and 9 responding and non-responding patients respectively.

As shown in Supp. table 1, responders significantly reduced CRP, already at W2 post first treatment while non-responders presented a trend of reduced CRP at W2, but their CRP level following 14 weeks was elevated and significantly higher than CRP level in responders. No significant difference was found in target TNF α levels, neither in responders or non-responders, as measured by either serum cytokine level using Luminex or by adjusted gene expression. As expected, IFX drug levels were shown to be significantly reduced, in both responders and non-responders at W14 compared to W2, due to the transition from induction to maintenance therapy. Drug levels of responders were significantly higher compared to non-responders at W14. However, at W2, no significant difference in drug levels was measured. Responders

also showed improved albumin levels along treatment, with significantly higher levels compared to non-responders at W14. All other parameters were comparable between the two response groups.

Validation real life IBD cohort

The validation cohort consisted of 29 CD patients from the RHCC, which were classified to 20 and 9 clinical responding and non-responding respectively patients according to the above-described decision algorithm (Supp. table 9).

CyTOF sample processing and analysis

A total of 2×10^6 cells of each sample were stained (1 h; room temperature) with a mixture of metaltagged antibodies (complete list of antibodies and their catalog numbers is provided in Supp. table 2). This mix contained antibodies against phenotyping markers of the main immune populations and some central cytokine and chemokine receptors. All antibodies were validated by the manufacturers for flow application (as indicated on the manufacturer's datasheet, available online) and were conjugated by using the MAXPAR reagent (Fluidigm Inc.). Iridium intercalators were used to identify live and dead cells. The cells were fixed in 1.6% formaldehyde (Sigma-Aldrich) at 4°C until they were subjected to CyTOF mass cytometry analysis on a CyTOF I machine (Fluidigm Inc.). Cell events were acquired at approximately 500 events/s. To overcome potential differences in machine sensitivity and a decline of marker intensity over time, we spiked each sample with internal metal-isotope bead standards for sample normalization by CyTOF software (Fluidigm Inc.) as previously described⁴³.

For data preprocessing, the acquired data were uploaded to the Cytobank web server (Cytobank Inc.) to exclude dead cells and bead standards. The processed data were analyzed using Citrus algorithm, which performs hierarchical clustering of single cell-events by a set of cell-type defining markers and then assigns per sample, per cluster its relative abundance in each sample as well as the median marker expression for each functional marker per cluster⁴⁴. Citrus analysis was applied separately on PBMCs and Granulocytes population in each sample using the following parameters: minimum cluster size percentage of 0.01 and 0.02 for PBMCs and Granulocytes respectively, subsampling of 15,000 events per sample and arcsin hyperbolic transform cofactor of 5. The gating for the classification of the clusters is detailed in Supp. table 3.

Blood transcriptome analysis

Whole blood was maintained in PAXgene Blood RNA tubes (PreAnalytiX). RNA was extracted and assayed using Affymetrix Clariom S chips (Thermo Fisher Scientific). The microarray data are available at the Gene Expression Omnibus database (http://www.ncbi.nlm.nih.gov/geo/). The raw gene array data were processed to obtain a log2 expression value for each gene probe set using the RMA (robust multichip average) method available in the affy R package. Probe set annotation was performed using affycoretools and clariomshumantranscriptcluster.db packages in R. Data were further adjusted for batch effect using empirical Bayes framework applied by the Combat R package.

Gene expression data were further adjusted for variations in frequency of major cell types across samples as measured by CyTOF, including CD4+ T cells, CD8+ T cells, CD19+ B cells, NK cells, monocytes and granulocytes, to allow detection of differential biological signals that do not stem from cell proportion

- 441 differences, which might be otherwise masked in unadjusted gene expression data. Adjustment was
- 442 performed using the CellMix R package.

476

477

Cytokines and chemokines measurement using Luminex bead-based multiplex assay

- 444 Serum was separated from whole blood specimens and stored at -80°C until used for cytokine
- determination. Samples were assayed in duplicate according to the manufacturers' specifications
- 446 (ProcartaPlex™ Immunoassay, EPX450-12171-901, eBioscience, Cytokine/Chemokine/Growth Factor 45-
- 447 Plex Human Panel 1, Supp. table 4).
- Data were collected on a Luminex 200 instrument and analyzed using Analyst 5.1 software (Millipore) and
- 449 NFI (Median Fluorescence Intensity) values were used for further data processing. A pre-filtering was
- 450 applied as follows: samples with low mean bead count, below 50 were excluded from analysis. In addition,
- duplicates with high CV values (Coefficient of variation) above 40% were omitted. NFI values with low
- bead count, below 20 were filtered out, but in cases which one replicate had acceptable bead count and
- the CV values for both replicates were less than 25%, NFI values were retained.
- 454 Finally, net MFI values were calculated by blank reduction followed by log2 transformation. Data were
- further adjusted for batch effect using the empirical Bayes framework applied by the Combat R package.

456 Characterization of IFX responders and non-responders' dynamics through integrative molecular

- 457 response axis combining external and in-house data
- 458 An integrative molecular response axis was constructed to recapitulate the complex nature of anti-TNFα
- 459 response progression dynamics which enables to track individual immune dynamics of both responding
- and non-responding patients. This methodology was assessed using an external data-based axis.
- 461 For unbiased definition of the 'Health axis' and validation of our own data we used public gene expression
- data of whole blood from 25 UC patients and 50 CD patients in active or inactive disease states, available
- in Gene Expression Omnibus (GSE94648). The patients in this external cohort were treated with different
- 464 medications including 5-ASAs, Immunosuppressants, anti-TNF agents, steroids and combinations of these
- therapies, as previously described⁴⁵, representative of a relatively large portion of the treated IBD patient
- 466 population. The analysis was performed in several steps: (1) Differential expression analysis between
- active disease and healthy states for UC and CD separately (Supp. Table 5), using the limma R package,
- 468 followed by PCA (Principal Component Analysis). (2) Ordinal lasso was used to select the principal
- components that best describe the desired directionality from active through inactive to healthy state,
- based on optimal absolute coefficient values and percentage of variance explained parameters (Supp.
- Table 6). (3) The 'Health axis' coordinates were defined based on initial and terminal points determined
- as the mean of the two end-point coordinates of active and healthy states. (4) Applying vector
- 473 multiplication (dot product) for the calculation of the projection of sample vector from our in-house
- cohort in the direction of the external 'health axis', to estimate sample position on the axis. (5) Evaluation
- of the distance of patient samples between two time points based on sample axis location.

Multi-omics network of anti-TNF blood response dynamics

Core co-expression response network

To identify features that change over time in responders, a linear mixed-effects model was used, in which time was treated as a fixed effect and individuals were treated as a random effect (Imer R package) to allow testing differential expression by time while accounting for between-subject variations. P-values were calculated empirically through a permutation test (n perm=1000). In each permutation, feature measurements were shuffled between visits for each responding patient. Permutation based p-values were obtained by comparing the absolute value of the non-permuted β coefficient for each feature to the null distribution of permuted β coefficients for the same feature. In order to calculate FDR based on the permutation results, permuted p-value was determined for each permuted β coefficient, by comparing the tested permuted β coefficient to the distribution of the other permuted β coefficients for each feature. Then FDR was estimated by comparing the non-permuted p-values to the null distribution of the permuted β -values. A similar calculation was performed for non-responders (max n perm =512).

In addition to the determination of dynamic features in the full responders' sample data, a random subsampling of samples from the responders group, without replacement, was applied to achieve equal sample size between responders and non-responders. Two-hundred subsamples were generated and tested using linear mixed-effects models. In this part, for the comparison of equally sized responders and non-responders' groups, p-values were calculated based on the t-statistic using the Satterthwaite approximation, implemented in the ImerTest R package, followed by multiple hypotheses correction using the Benjamini-Hochberg procedure.

Co-expression network based on V1-V2 fold-change expression values of the significantly altered features (FDR<0.15) was constructed, based on pairwise Spearman's rank correlation using the psych R package. Filtering was applied to remove feature-pairs with insignificant correlation with a cutoff of FDR<0.1.

Network propagation

Network propagation procedure was applied to enhance the biological signal of the obtained networks as previously described ⁴⁶ with slight modifications. Briefly, for each node in the network, protein interactors with a combined score above 700 were extracted based on STRING database (functional protein association networks; https://string-db.org/cgi/download.pl) using STRINGdb R package. A node interactor was added as a linker gene to the network if its own interactors (hubs) were significantly enriched in the core network features. Enrichment was calculated using the hypergeometric test in the stats R package. Calculated p-values were adjusted for multiple hypotheses using the Benjamini-Hochberg procedure. A cutoff of FDR<0.05 was selected for significant enrichment of the tested interactor hubs in the immune network.

Functional enrichment assessment for the response network

To assess dynamics in the functional level, genes were grouped to functional sets by using a semi-supervised approach combining both network structure and known gene set annotations from Hallmark, Kegg, Reactome, Biocarta, PID and BP Go terms. Each edge in the network was classified to a specific pathway if its two linked nodes were annotated in the same biological group. Pathways with less than 5 mapped edges were filtered out. This was followed by a global gene set enrichment analysis using fGSEA (FDR<0.15, nperm=1000, minSize=10, maxSize=400).

The dynamic enriched pathway structures were further tested for significance by comparing the density (graph density score) of each pathway associated sub-network to a parallel sub-network density obtained

from 100 random networks with a matched size according to the Erdos-Renyi model which assigns equal

probability to all graphs with identical edge count (igraph R package). P-value was evaluated as the

522 proportion of random module density scores that were higher than the real module density score.

523 Additional filtering was applied according to the number of connected components in a pathway sub-

graph (igraph R package). Only highly connected pathways (percentage of largest connected

525 component>50%, size of the connected component>10) were included.

The dynamic pathways list was further condensed by filtering out high overlapping pathways using Jaccard

index. Accordingly, in overlapping pathways pairs that presented a Jaccard index above 0.5 the smaller

module was omitted.

To further associate the assigned pathways with treatment response, the Wilcoxon test was used to compare V1 to V2 and V1 to V3 relative pathway scores in responders and non-responders. p-values were adjusted for multiple hypotheses using the Benjamini-Hochberg procedure (FDR<0.05). Relative pathway scores were calculated for each sample as previously described ^{38,47} (see Relative pathway score evaluation). To assess cellular contributions for each pathway, the non-adjusted expression of each gene in the dynamic pathways was regressed over the major peripheral cell type frequencies as determined by CyTOF including granulocytes, CD4 and CD8 T cells, B cells, NK cells and monocytes. The cell-specific contribution to each pathway was determined as the mean of the coefficients of the tested cell type across all genes in the module. The centrality of each pathway in the response network was also evaluated by calculating the pathway based mean betweenness and degree across all gene members of the pathway (igraph R package). To further assess the clinical relevance of the dynamic pathways to the treatment response, the calculated pathway score at all tested time points was correlated with CRP using Spearman's rank correlation test.

Relative pathway score evaluation

The expression of each gene in the pathway was standardized by the z-score transformation, to enable comparable contribution of each gene member to the pathway score, followed by mean value calculation across the transformed genes in the pathway for each sample.

'Disruption Networks' framework

To understand individual variation in non-response dynamics, we developed an approach termed 'Disruption Networks' in which individual non-responders are iteratively added to the obtained normal IFX response network, and the disruption in the correlation structures is assessed for each edge in the reference response network. The disruption is evaluated in the node (gene/cell) or the module level to determine biological mechanisms that may explain patterns of the non-response.

More specifically, consider a feature matrix $F_{n\times m}$ where n is the number of samples for a given condition, in our case, n is the number of samples of responding patients and m is the number of features, where f(i,j) refers to a fold change measured value at a given time point relative to baseline, of the j-th feature in the i-th sample. Let matrix $R_{m\times m}$ be the feature pairwise Spearman's rank correlation matrix based on F which represents the global response network, where r(j,k)=cor(j,k) for genes j and k. Insignificant correlation values according to FDR thresholds, as described above, were presented as NAs in the matrix.

The 'Disruption Networks' construction was assessed individually for each non-responder as follows: a new $F'_{(n+1)} \times m$ matrix was generated by the addition of the tested non-responder to the responders' samples. Based on F', a new pairwise Spearman's rank correlation matrix was calculated to obtain $R'_{m \times m}$,

- in which r'(j,k) is the correlation between j and k genes when including the non-responder in the
- responders' samples.

593

594

595 596

597

598

- For correlation coefficients comparison, correlation coefficient values were transformed using Fisher z-
- transformation by the following formula:
- 565 $z(r) = 0.5*ln(\frac{1+r}{1-r})$ and a standard error of $SEz(r) = \frac{1}{\sqrt{n-3}}$ where n is the number of samples.
- We define a 'disruption' term as the drop in the Fisher z transformed values between two genes as a result
- of the non-responder addition using the statistical z score which is defined as:

568
$$disruption(j,k) = z \ score = \frac{z(r')-Z(r)}{Pooled.SEz} = \frac{z(r')-Z(r)}{\sqrt{\frac{1}{(n+1)-3} + \frac{1}{n-3}}}.$$

- Only negative values of sign(r*(z(r')-Z(r))), which indicate weakening of the original 569 correlation obtained in responders were included, while positive values were set to zeros. Drop degree of 570 571 confidence for non-responders was assessed empirically for each drop value in each edge, based on the 572 non-responder drop value percentile in the responders' normal drop distribution. This was further 573 corrected for multiple testing using the Benjamini-Hochberg procedure. Edges with drop adjusted percentile <0.1 were considered as significantly disrupted. Insignificant drop values were set to zeros. 574 575 Analysis of disruption parameters in the feature level, revealed a considerably expansion of the detected differential signal between response groups, compared to standard differential analysis by Wilcoxon test. 576 While using the Wilcoxon test we detected only one feature (0.06%), with significant differential dynamics 577 between response groups at W2, we identified this feature together with 179 additional features (10%) 578 579 when using disruption parameter of top mean drop intensity (FDR<0.1 by Wilcoxon test, FDR<0.1 for significant dropout and top 0.1 percentile of mean drop intensity, Figure 3b). We observed similar results 580 581 for the disrupted edge ratio (0.06% Vs. 14.4% significant features identified by Wilcoxon test (FDR<0.1) and top disrupted edge ratio parameter (FDR<0.1 for significant dropout and top 0.1th percentile of node 582 disrupted edges) respectively, Supp. figure 4a). Testing the agreement of both disruption parameters, we 583 identified 9.4% dynamics differential features including the single feature identified by Wilcoxon test 584 585 (Supp. figure 4b).
- Disruption was also measured in the pathway level for each individual using three different measurements: (1) Pathway specific mean drop intensity in which a mean drop intensity was calculated across the relevant edges in the module, for a specific individual. (2) Pathway specific percentage of disrupted edges which determines the percentage of edges in the pathway that the specific individual is significantly disrupted in. (3) Pathway specific percentage of disrupted nodes which evaluate the percentage of disrupted nodes for a specific individual out of all module nodes.
 - For binary classification of disrupted pathways, we quantify the disruption measure across a range of percentile values in each parameter. For each parameter, in each percentile, the selected positive disrupted modules were those that were disrupted in at least 50% of the non-responding patients and in less than 20% of the responders, or in cases where the difference between the percentage of disrupted non-responders to responders is higher than 50%. The top significantly positive disrupted modules were defined as those with a complete agreement of all three parameters in the highest percentile with shared selected pathways across all parameters, which in our case was determined as the 0.8 percentile.

Single cell RNA sequencing

Peripheral blood mononuclear cells (PBMCs) cryopreservation and thawing

Blood samples were drawn before IFX first infusion. PBMCs were isolated using density gradient centrifugation by spinning blood over UNI-SEPmaxi+ tubes (Novamed Ltd.) following the manufacturer's protocol. Isolated cells were resuspended in 1 ml freezing solution, containing 10% DMSO and 90% FCS. The samples were kept in Nalgene Mr. Frost® Cryo 1°C Freezing Container (ThermoFisher scientific) with Isopropyl alcohol at -80°C over-night, and immediately after placed in a liquid nitrogen container for long-term storage.

For thawing, frozen PBMCs were immediately transferred to a water bath at 37°C for 2-3 min, until a tiny ice crystal was remained. Thawed cells were transferred into 50 mL centrifuge tubes and rinsed with 1 mL of warm (37 °C) RPMI 1640 supplemented with 10% of FCS which was added dropwise to the DMSO containing fraction while gently shaking the cells. Next, the cells were sequentially diluted by first adding 2 mL of medium followed by another 4, 8 and 16 mL respectively with 1 min wait between the four dilution steps. The diluted cell suspension was centrifuged for 5 min at 300 g. Most of the supernatant was discarded leaving ~1 ml, and the cells were resuspended in 9 ml of medium followed by additional centrifugation for 5 min at 300 g and resuspended with the same media to reach the desired cell concentration.

Single cell RNA sequencing in 10X genomics platform

PBMCs from responder and non-responder patients pre-treatment (N=2) were prepared for scRNA-seq according to the 10x Genomics Single Cell protocols for fresh frozen human peripheral blood mononuclear cells (see above for cell preservation and thawing). The cells were adjusted to a final cell concentration of 1000 cells/UI and placed on ice until loading into the 10x Genomics Chromium system. The scRNA sequencing was performed in the genomic center of the biomedical core facility in the Rappaport faculty of medicine at the Technion - Israel Institute of Technology. Libraries were prepared using 10x Genomics Library Kits (Chromium Next GEM Single Cell 3' Library & Gel Bead Kit v3.1, PN-1000121) using 20,000 input cells per sample. Single cell separation was performed using the Chromium Next GEM Chip G Single Cell Kit (PN-1000120). The RNAseq data was generated on Illumina NextSeq500, high-output mode (Illumina, FC-404-2005), 75 bp paired-end reads (Read1- 28 bp, Read2- 56 bp, Index- 8 bp).

Single cell data analysis

Cell Ranger single cell software suite was used for sample de-multiplexing, alignment to human reference genome (GRCh38-3.0.0), cell barcode processing and single cell UMI counting following default settings. The UMI count matrix was further processed using the Seurat R package (version 3.1.4). First, as a QC step, cells that had a unique feature count of less than 200 were filtered out. Additional filtering was applied to remove features detected in less than 3 cells. we further filtered cells based on mitochondrial gene content above 0.25%. After this step, 19275 single cells and 20673 genes in total were retained and included in downstream analyses. This was followed by Global-scaling library size normalization. Genes were scaled in comparison to all other cells and regressed out the effects of unwanted sources of variation including UMI counts and percentage of mitochondrial genes for the remaining cells. At the next step, we performed linear dimensionality reduction on the scaled data of the top 2000 highly variable genes. Resampling test based on the jackstraw procedure and Elbow plot were performed to identify the first 30 significance principal components that were used for downstream visualization by t-SNE plot.

- SingleR was used to annotate cell types based on correlation profiles with two different resolutions of cell classification using the Blueprint-Encode⁴⁸ and the Monaco Immune Cell⁴⁹ reference datasets of pure cell types. Differential expression analysis between responders and non-responders was performed for each cell population using a Wilcoxon Rank Sum test implemented in the FindAllMarkers function in the Seurat package.
- Relative pathway score based on the expended fiber-organization baseline differential genes was calculated for each single cell and compared between cell subsets and response groups using Wilcoxon test (for the expended fiber organization differential genes assessment see below description for selection and evaluation of predictive model for IFX treatment response; see the above description for relative pathway score calculation).
- 650 To identify cell specific enriched pathways that are associated with the predictive fiber-organization related signature, we constructed a co-expression network based on the pre-treatment expression of the 651 652 predictive genes: RAC1, PAK1, ICAM1, LYN, FCGR3A and IL-1β, in intermediate monocyte subset in each response group using the MTGOsc R package (Spearman's correlation, thinning net by 0.1 top percentile). 653 Functional enrichment analysis was performed based on the co-expressed network nodes, by a 654 655 hypergeometric test based on the Reactome database using the Clusterprofiler R package (P-adjust<0.05). 656 Wilcoxon test was assessed to identify significant differences in pathway scores between response groups 657 for each enriched pathway in each monocyte subset. P-values were further adjusted for multiple testing 658 using the Benjamini-Hochberg procedure.

Predictive model for IFX treatment response

659

660

661

662

663

664 665

666 667

668

669 670

671

672

673

681

Given the significant linkage between monocytes and the differential fiber organization pathway, in order to build a cell specific pre-treatment classifier, we expanded the fiber organization adjusted-bulk based genes through intersection of knowledge based-(combined 9606.protein.links.detailed.v11.0 from the STRING protein interaction database: http://string-db.org/ and data-driven networks (Monocytes single-cell based co-expression from a representative responder and non-responder patients at baseline, Spearman's r, thinning percentile: 0.05, MTGOsc R package). This yielded a combined network of 42 edges containing 23 nodes. To build a predictive signature, we used elastic net regularized logistic regression for predictors selection, which has the advantage of including all correlated predictors sharing transcriptional signal (grouping effect), rather than selecting one variable from a group of correlated predictors while ignoring the others⁵⁰. We used the glmnet R package implemented within the caret R package for model fitting by tuning over both alpha (ranging from 0.5-1, n=6) and lambda (ranging from 0.0001-1, n=20) parameters with 100 repeated 2-fold cross-validation. The optimized model was chosen based on the best performance value using the Receiver operating characteristic (ROC) metric (alpha=0.5, lambda=0.26).

- After variable selection, we calculated AUC based on relative pathway score combining the selected genes using the pROC R package.
- Internal validation was performed by bootstrapping (n=1000 bootstrap samples) for the AUC by randomly drawing subjects with the same sample size from the original cohort (with replacement).
- A permutation test was used for estimating one-tailed P-value (n=10000 permutations) by shuffling the subject labels between the response groups and the expression of the selected signature genes. Then we tested the null hypothesis that the observed AUC was drawn from this null distribution.

External validation of the predictive signature using additional independent real-life IBD cohort

For independent validation of the predictive signature, we used an independent IBD cohort of 29 patients (see Patient in the validation real life cohort). RNA was then extracted using RNeasy mini kit (QIAGEN) according to the manufacturer's instruction (for preservation and thawing of PBMCs see Peripheral blood mononuclear cells (PBMCs) cryopreservation). Complementary DNA was synthesized using Maxima first strand cDNA synthesis kit with dsDNase (Thermo Scientific). qPCR was performed using 7300 Real-Time PCR System (AB Applied Biosystems). Relative cytokine expression was calculated following normalization to glyceraldehyde-3 phosphate dehydrogenase (GAPDH) expression (Supp. table 10 for the PCR primer sets). Primers were purchased from Sigma Aldrich. The expression of the genes in the predictive signature was calculated relative to CD14 expression, to measure monocytes' centered differential expression between response groups pre-treatment. Relative pathway score was used to assess prediction performance (see Relative pathway score evaluation).

Assessment of the predictive signature performance in RA

The prediction performance of the RAC1-PAK1 signature in RA public expression datasets was evaluated using the following datasets: GSE20690 (n=68 of which 43 and 25 are responders and non-responders respectively), GSE33377 (n=42 of which 18 and 24 are responders and non-responders respectively) and GSE42296 (n=19 of which 13 and 6 are responders and non-responders respectively).

Gene expression was adjusted to major cell type contributions (see Blood transcriptome analysis), which were evaluated by deconvolution using a linear regression framework in which individual samples were regressed based on a characteristic expression of marker genes expressed in 17 cell-types (CellMix R package). This was followed by performance prediction calculation for each study based on the relative signature score based on the adjusted gene expression. Due to differences in expression platforms between studies, there were genes in the signature which were not present in a specific dataset, therefore those genes were not used in the calculation of the relative signature score for the prediction of the specific study. To combine prediction performance from these independent studies we constructed a summary ROC curve (meta-ROC) using the nsROC R package which performs a simple linear interpolation between pairs of points of each individual ROC.

Acknowledgments

710

714

723

729

- 711 This work was supported by funding of the Helmsley Charitable Trust to Y.C and S.S.S-O. We thank
- 712 T.Shvedov for contribution to patient enrollment and clinical data collection. S.Pollok, L.Pinzur,
- 713 N.Molshatzki and Y.Benita for fruitful discussions and advice on the computational methodology.

Author contributions

- 5.S.S.-O, Y.C. conceived the idea; S.S.S-O, Y.C, S.G.V, E.S and R.G designed the analyses, S.S.S-O, Y.C. and
- 716 S.G.V performed the interpretation; S.G.V and R.G performed the design and development of the
- 717 computational pipeline and validation; A.K, B.P, Y.G and A.A performed development of the
- 718 computational methodology; N.Ma, A.B, S.P and E.S counseled regarding the biological interpretation; E.S
- performed the experimental design of the collected cohort and E.S, N.Ma, A.A and T.D performed the
- data generation; A.B and N.Mi performed the experimental validation; A.B, S.P performed the sample
- 721 collection; Y.C, H.B.Y and Y.G performed patient enrollment and clinical characterization; S.S.S-O, Y.C and
- 722 S.G.V wrote the manuscript.

Competing interests

- 724 These authors disclose the following: Y.C received consulting fees from AbbVie, Janssen, Takeda, Pfizer
- and CytoReason; speaker fees from AbbVie, Janssen, and Takeda; and grants from AbbVie, Takeda and
- Janssen. S.S.S-O received grant fees from Takeda, S.S.S.-O, E.S. and R.G declares CytoReason equity and
- advisory fees. N. Ma and A.K are employees at CytoReason. S.G.V declares CytoReason advisory fees. The
- 728 remaining authors disclose no conflicts.

References

730 731

- 732 1. Jiang, P. *et al.* Signatures of T cell dysfunction and exclusion predict cancer immunotherapy response. *Nat. Med.* (2018). doi:10.1038/s41591-018-0136-1
- 734 2. Murthy, S. K. *et al.* Introduction of anti-TNF therapy has not yielded expected declines in hospitalisation and intestinal resection rates in inflammatory bowel diseases: A population-based interrupted time series study. *Gut* (2020). doi:10.1136/gutjnl-2019-318440
- 3. Berns, M. & Hommes, D. W. Anti-TNF-α therapies for the treatment of Crohn's disease: the past, present and future. *Expert Opin. Investig. Drugs* (2015). doi:10.1517/13543784.2016.1126247
- Mitoma, H., Horiuchi, T., Tsukamoto, H. & Ueda, N. Molecular mechanisms of action of anti-TNF-α agents Comparison among therapeutic TNF-α antagonists. *Cytokine* (2018).
 doi:10.1016/j.cyto.2016.08.014
- Roda, G., Jharap, B., Neeraj, N. & Colombel, J. F. Loss of Response to Anti-TNFs: Definition,
 Epidemiology, and Management. *Clinical and Translational Gastroenterology* (2016).
 doi:10.1038/ctg.2015.63
- 745 6. Seymour, H. E., Worsley, A., Smith, J. M. & Thomas, S. H. L. Anti-TNF agents for rheumatoid arthritis. *Br. J. Clin. Pharmacol.* (2001). doi:10.1046/j.1365-2125.2001.00321.x
- 7. Digby-Bell, J. L., Atreya, R., Monteleone, G. & Powell, N. Interrogating host immunity to predict treatment response in inflammatory bowel disease. *Nature Reviews Gastroenterology and Hepatology* (2020). doi:10.1038/s41575-019-0228-5
- West, N. R. *et al.* Oncostatin M drives intestinal inflammation and predicts response to tumor necrosis factor–neutralizing therapy in patients with inflammatory bowel disease. *Nat. Med.* **23**, 579–589 (2017).
- 9. Gaujoux, R. *et al.* Cell-centred meta-Analysis reveals baseline predictors of anti-TNFα non-response in biopsy and blood of patients with IBD. *Gut* **68**, 604–614 (2019).
- 755 10. Mulhearn, B., Barton, A. & Viatte, S. Using the immunophenotype to predict response to biologic drugs in rheumatoid arthritis. *Journal of Personalized Medicine* (2019). doi:10.3390/jpm9040046
- 757 11. Kuijjer, M. L., Tung, M. G., Yuan, G. C., Quackenbush, J. & Glass, K. Estimating Sample-Specific Regulatory Networks. *iScience* (2019). doi:10.1016/j.isci.2019.03.021
- 12. Liu, X., Wang, Y., Ji, H., Aihara, K. & Chen, L. Personalized characterization of diseases using sample-specific networks. *Nucleic Acids Res.* (2016). doi:10.1093/nar/gkw772
- 13. Liu, Y. *et al.* Cytokine-mediated regulation of activating and inhibitory Fcγ receptors in human
 762 monocytes. *J. Leukoc. Biol.* (2005). doi:10.1189/jlb.0904532
- 763 14. Turner, M. & Billadeau, D. D. VAV proteins as signal integrators for multi-subunit immune-764 recognition receptors. *Nature Reviews Immunology* (2002). doi:10.1038/nri840
- 765 15. Zhao, X., Carnevale, K. A. & Cathcart, M. K. Human Monocytes Use Rac1, Not Rac2, in the NADPH Oxidase Complex. *J. Biol. Chem.* (2003). doi:10.1074/jbc.M302208200
- 767 16. Parikh, K. *et al.* Suppression of p21Rac signaling and increased innate immunity mediate remission in Crohn's disease. *Sci. Transl. Med.* (2014). doi:10.1126/scitranslmed.3006763
- 769 17. Kapellos, T. S. *et al.* Human monocyte subsets and phenotypes in major chronic inflammatory 770 diseases. *Frontiers in Immunology* (2019). doi:10.3389/fimmu.2019.02035
- 771 18. Tanino, M. *et al.* Prediction of efficacy of anti-TNF biologic agent, infliximab, for rheumatoid 772 arthritis patients using a comprehensive transcriptome analysis of white blood cells. *Biochem.* 773 *Biophys. Res. Commun.* (2009). doi:10.1016/j.bbrc.2009.06.149
- Toonen, E. J. M. *et al.* Validation study of existing gene expression signatures for anti-TNF treatment in patients with rheumatoid arthritis. *PLoS One* (2012).
 doi:10.1371/journal.pone.0033199
- 777 20. Mesko, B. *et al.* Peripheral blood derived gene panels predict response to infliximab in 778 rheumatoid arthritis and Crohn's disease. *Genome Med.* (2013). doi:10.1186/gm463
- 779 21. Kalliolias, G. D. & Ivashkiv, L. B. TNF biology, pathogenic mechanisms and emerging therapeutic strategies. *Nat. Rev. Rheumatol.* (2016). doi:10.1038/nrrheum.2015.169

- Lügering, A. et al. Infliximab induces apoptosis in monocytes from patients with chronic active
 Crohn's disease by using a caspase-dependent pathway. Gastroenterology (2001).
 doi:10.1053/gast.2001.28702
- 784 23. Batko, B., Schramm-Luc, A., Skiba, D. S., Mikolajczyk, T. P. & Siedlinski, M. TNF-α inhibitors
 785 decrease classical CD14 hi cd16– monocyte subsets in highly active, conventional treatment
 786 refractory rheumatoid arthritis and ankylosing spondylitis. *Int. J. Mol. Sci.* (2019).
 787 doi:10.3390/ijms20020291
- 788 24. Rossol, M. *et al.* Interaction between Transmembrane TNF and TNFR1/2 Mediates the Activation of Monocytes by Contact with T Cells. *J. Immunol.* (2007). doi:10.4049/jimmunol.179.6.4239
- 790 25. Yokoyama, Y. *et al.* Efficacy of granulocyte and monocyte adsorptive apheresis in patients with inflammatory bowel disease showing lost response to infliximab. *J. Crohn's Colitis* (2020). doi:10.1093/ecco-icc/jjaa051
- 793 26. Marei, H. & Malliri, A. Rac1 in human diseases: The therapeutic potential of targeting Rac1 signaling regulatory mechanisms. *Small GTPases* (2017). doi:10.1080/21541248.2016.1211398
- 795 27. Muise, A. M. *et al.* Single nucleotide polymorphisms that increase expression of the guanosine 796 triphosphatase RAC1 are associated with ulcerative colitis. *Gastroenterology* (2011). 797 doi:10.1053/j.gastro.2011.04.057
- 798 28. Tiede, I. *et al.* CD28-dependent Rac1 activation is the molecular target of azathioprine in primary human CD4+ T lymphocytes. *J. Clin. Invest.* (2003). doi:10.1172/JCI16432
- Lim, S. Z. & Chua, E. W. Revisiting the role of thiopurines in inflammatory bowel disease through
 pharmacogenomics and use of novel methods for therapeutic drug monitoring. Frontiers in
 Pharmacology (2018). doi:10.3389/fphar.2018.01107
- 30. Hamerman, J. A., Ni, M., Killebrew, J. R., Chu, C. L. & Lowell, C. A. The expanding roles of ITAM
 804 adapters FcRγ and DAP12 in myeloid cells. *Immunological Reviews* (2009). doi:10.1111/j.1600-065X.2009.00841.x
- 806 31. Louis, E. *et al.* Association between polymorphism in IgG Fc receptor IIIa coding gene and biological response to infliximab in Crohn's disease. *Aliment. Pharmacol. Ther.* (2004). doi:10.1111/j.1365-2036.2004.01871.x
- 809 32. Moroi, R. *et al.* FCGR3A-158 polymorphism influences the biological response to infliximab in Crohn's disease through affecting the ADCC activity. *Immunogenetics* (2013). doi:10.1007/s00251-013-0679-8
- 812 33. McRae, B. L. *et al.* Fc receptor-mediated effector function contributes to the therapeutic 813 response of anti-TNF monoclonal antibodies in a mouse model of inflammatory bowel disease. *J. Crohn's Colitis* (2016). doi:10.1093/ecco-jcc/jjv179
- St. Chen, Y., Li, H., Lai, L., Feng, Q. & Shen, J. Identification of Common Differentially Expressed
 Genes and Potential Therapeutic Targets in Ulcerative Colitis and Rheumatoid Arthritis. Front.
 Genet. (2020). doi:10.3389/fgene.2020.572194
- Chen, J. Y. *et al.* Association of FCGR3A and FCGR3B copy number variations with systemic lupus erythematosus and rheumatoid arthritis in Taiwanese patients. *Arthritis Rheumatol.* (2014).
 doi:10.1002/art.38813
- Roberts, J. T., Patel, K. R. & Barb, A. W. Site-specific N-glycan Analysis of Antibody-binding Fc γ
 Receptors from Primary Human Monocytes. *Mol. Cell. Proteomics* (2020).
 doi:10.1074/mcp.RA119.001733
- Herter, S. *et al.* Glycoengineering of Therapeutic Antibodies Enhances Monocyte/Macrophage-Mediated Phagocytosis and Cytotoxicity. *J. Immunol.* (2014). doi:10.4049/jimmunol.1301249
- 826 38. Kotliarov, Y. *et al.* Broad immune activation underlies shared set point signatures for vaccine responsiveness in healthy individuals and disease activity in patients with lupus. *Nat. Med.* (2020). doi:10.1038/s41591-020-0769-8
- 39. Goh, K. Il *et al.* The human disease network. *Proc. Natl. Acad. Sci. U. S. A.* (2007).
 doi:10.1073/pnas.0701361104
- 831 40. Singh, S., George, J., Boland, B. S., Casteele, N. Vande & Sandborn, W. J. Primary non-response to

- tumor necrosis factor antagonists is associated with inferior response to second-line biologics in patients with Inflammatory bowel diseases: A systematic review and meta-analysis. *J. Crohn's Colitis* (2018). doi:10.1093/ecco-jcc/jjy004
- Rosen, M. J., Minar, P. & Vinks, A. A. Review article: Applying pharmacokinetics to optimise dosing of anti-TNF biologics in acute severe ulcerative colitis. *Alimentary Pharmacology and Therapeutics* (2015). doi:10.1111/apt.13175
- Sarikaya, I. *et al.* Tc-99m dextran and Tc-99m HIG findings in patients with ulcerative colitis. *Clin. Nucl. Med.* (1999). doi:10.1097/00003072-199904000-00005
- Finck, R. *et al.* Normalization of mass cytometry data with bead standards. *Cytom. Part A* (2013). doi:10.1002/cyto.a.22271
- 842 44. Bruggner, R. V., Bodenmiller, B., Dill, D. L., Tibshirani, R. J. & Nolan, G. P. Automated 843 identification of stratifying signatures in cellular subpopulations. *Proc. Natl. Acad. Sci. U. S. A.* 844 (2014). doi:10.1073/pnas.1408792111
- 845 45. N., P. *et al.* Usefulness of transcriptional blood biomarkers as a non-invasive surrogate marker of mucosal healing and endoscopic response in ulcerative colitis. *J. Crohn's Colitis* (2017). doi:10.1093/ecco-icc/jjx091 LK -
- http://sfx.cineca.it:9003/unito?sid=EMBASE&sid=EMBASE&issn=18764479&id=doi:10.1093%2Fe cco-jcc%2Fjjx091&atitle=Usefulness+of+transcriptional+blood+biomarkers+as+a+non-
- invasive+surrogate+marker+of+mucosal+healing+and+endoscopic+response+in+ulcerative+coliti s&stitle=J.+Crohn%27s+Colitis&title=Journal+of+Crohn%27s+and+Colitis&volume=11&issue=11& spage=1335&epage=1346&aulast=Planell&aufirst=N%C3%BAria&auinit=N.&aufull=Planell+N.&co den=&isbn=&pages=1335-1346&date=2017&auin
- 46. Li, S. *et al.* Molecular signatures of antibody responses derived from a systems biology study of five human vaccines. *Nat. Immunol.* **15**, 195–204 (2014).
- Tsang, J. S. *et al.* Global analyses of human immune variation reveal baseline predictors of postvaccination responses. *Cell* (2014). doi:10.1016/j.cell.2014.03.031
- 48. Fernández, J. M. *et al.* The BLUEPRINT Data Analysis Portal. *Cell Syst.* (2016).
 48. doi:10.1016/j.cels.2016.10.021

- 860 49. Xu, W. *et al.* Mapping of γ/δ T cells reveals Vδ2+ T cells resistance to senescence. *EBioMedicine* (2019). doi:10.1016/j.ebiom.2018.11.053
- So. Zou, H. & Hastie, T. Regularization and variable selection via the elastic net. *J. R. Stat. Soc. Ser. B*Stat. Methodol. (2005). doi:10.1111/j.1467-9868.2005.00503.x

Figure titles and legends

865

866

867

868

869

870

871

872

873

874

875

876

877

878

879

880

881

882

883

884

885 886

887

888

889

890

891

892

893

894

895

896

897

898

899

900

901

902

903

904

905

906

907

908

909

910

911

912

Fig 1| External data-driven disease specific molecular response metric, termed 'health axis', indicated that responders exhibit a trajectory of treatment-induced immune dynamics while non-responders exhibit an overall opposite direction. a, Overview of the 'health axis' analysis. b, 'Health axis' assessment. Left panel, external public (GSE94648) based 'health axis' which defines a transition from IBD active disease through inactive disease to healthy state by PCA based differential expressed genes between disease/health states. Right panel, the projection distance of responding and non-responding patients' samples from our real-life cohort on the 'health axis' at W2 compared to baseline. c, Boxplots comparing responders' and non-responders' projection dynamics on the 'health axis' at each treatment interval (One-tailed permutation P-values shown, n=10000). d, Scatterplot of the relationship between progress on the 'health axis' between W2 to baseline and between W2 to W14 (n=23, Spearman's r=-0.44, P<0.1).

Fig 2 | Normal infliximab dynamics correlated with changes in monocytes and reduced expression of innate immune related pathways. a, Cell frequency alterations following IFX treatment. Left panel, PCA presenting immune cell frequency changes following treatment based on 16 canonical immune populations determined by CyTOF. Arrow tail and head indicate the early W2 and later W14 relative to baseline compositional changes correspondingly. Ellipses represent the Euclidean distance from the center. Center panel, boxplots showing change in monocytes abundance following treatment relative to baseline in responders and non-responders (paired-Wilcoxon P-values shown). Right panel, scatterplot showing the relationship between changes in monocytes abundance (log transformed fold change relative to baseline) and changes in CRP (fold change relative to baseline) (n=23, Spearman correlation=0.4, P=0.01). b, Venn diagram showing dynamic features which significantly changed over time at 2 weeks and 14 weeks post treatment compared with baseline for each response group using linear mixed-effects models (FDR<0.15, n=1000 & n=519 permutations for responders and non-responders respectively). c, Scatterplot presenting the normal response network centrality of significantly enriched dynamic pathways at the early response period (GSEA, FDR<0.25, n perm=1000). Colors indicate pathway median fold change expression at the early response period relative to baseline in responders (colored dots denote significant change in relative pathway score by Wilcoxon test, FDR<0.05).

Fig 3| 'Disruption Networks' as a framework to perform sample level inferences to identify individual variation in drug response. a, 'Disruption Networks' concept, Left panel – a network is generated from a reference group (IFX responders) and then individual subjects from a test group (IFX non-responders) are iteratively added to the obtained response reference network, and the disruption in the correlation structure, defined as a dropout, is assessed for each patient across all edges. Right panel, representative highly disrupted edge demonstrating significant dropout values for non-responders. b, Feature specific differential signal between responders and non-responders dynamics at the early response period using disruption measurement of top mean drop intensity (x axis) and standard statistics by Wilcoxon test (y axis). c, 'Disruption Networks' statistic was aggregated across pathways to estimate sample specific disruption in the functional level, according to three parameters including percentage of disrupted edges, mean drop intensity and percentage of disrupted nodes. Heatmaps represent the disrupted dynamics in each parameter for each pathway and sample at W2 compared to baseline. Top significantly disrupted pathways are presented, defined as those with a complete agreement of all three parameters in the 0.8 percentile. Line graphs describe the percentage of disrupted patients in each response group. d, Distribution of degree and betweenness centrality for nodes belonging to the top disrupted pathways compared to other nodes in the network. Significance was determined using permutation test (n perm=10000). e, Meta disrupted pathway. Left panel, response network subgraph consist of nodes from the baseline differential disrupted pathways (FDR<0.1). Dimond shape and orange color represent cell frequency, circle shape represent cell centered expression. Red circles indicate the fiber organization pathway related central axis. Right panel, enrichment analysis of the disrupted pathways by hypergeometric test.

Fig. 4 | **Fiber-organization signaling, highly expressed in monocytes, predicts infliximab response at baseline. a**, Baseline expression differences in the disrupted pathways between response groups (NPMANOVA; bottom primary axis). Colors denote response network betweenness. The line graph represent correlation of changes in pathway score with changes in CRP (top secondary axis). **b**, The fiber organization differential nodes dynamics assessed by mean relative score across visits for each response group (Wilcoxon one-tailed P-values shown). **c**, Analysis of the cellular origin of the baseline differential fiber organization pathway using scRNA-seq analysis of PBMCs collected from representative responder and non-responder pre-treatment. Left panel, tSNE plot representing cell types identities annotated using singleR based on correlation profiles based on two reference datasets: the Blueprint-Encode and the Monaco Immune Cell datasets. Right panel, tSNE plot colored by the expended fiber organization scaled expression. The fiber organization baseline differential genes were expended through intersecting knowledge based (stringDB) and data-driven based (Monocyte single cell data) networks. **d**, The expended fiber organization scaled expression in the different monocyte subsets (Wilcoxon P-values shown). **e**, Mean mTNF expression in the different monocyte subsets as measured by CyTOF (Wilcoxon one-tailed P-values shown).

Fig. 5| Validation of the fiber organization predictive signature in an independent IBD cohort and three public RA cohorts pre IFX treatment. a, Baseline prediction of IFX response in the primary IFX cohort based on the expended fiber organization predictive signature score, in the cell adjusted space. Left panel, receiver operating characteristic (ROC) plots of 1000-bootsraps. The predictive signature was determined using elastic net (a=0.5, lambda=0.26, 100 repeated 2-fold CV) based on the adjusted baseline differential fiber organization related genes. Significance was determined by permutation test (n perm=10000). Right panel, boxplots of the fiber organization predictive signature score pre-treatment, in the different response groups in the cell-centered bulk expression. b, Validation of the pre-treatment predictive fiber organization signature in an additional independent cohort of 20 and 9 responders and non-responders respectively by qPCR. Gene values were normalized to CD14 expression for cell-centered values. Left panel, bar graph of the pre-treatment normalized expression of the signature genes and signature pathway score in each response group (Wilcoxon one-tailed P-values shown). Right panel, ROC based on the predictive signature relative score. c, Prediction performance of fiber organization signaling signature in RA public expression datasets. Left panel, boxplots comparing the fiber organization signature related genes and the pathway score between IFX RA responders (n=43) and non-responders (n=25) in a representative public dataset GSE20690 (Wilcoxon one-tailed P-values shown). Right panel, ROC based on the predictive signature relative score of the relevant cohort. d, Meta-ROC presenting the predictive performance of three independent public RA cohorts.

Supplemental Information titles and legends

- 948 Supp. Fig 1| CyTOF reveals multiple cell subset changes in responders following treatment and
- differences between response groups. a, Loading plot of PC2 based on major canonical cell composition
- changes at W2 and W14 compared to baseline. **b**, Cell-type specific alteration in cellular relative
- abundance during IFX treatment in responders and non-responders (paired-Wilcoxon P-values shown). c,
- 952 Correlation of cell abundance changes at W2 and W14 relative to baseline, with changes in CRP
- 953 (Spearman's correlation coefficients are shown, P-values are calculated by two tailed probability of the t-
- 954 statistic, P<0.05 for significant p-values).
- 955 Supp. Fig 2 | The cumulative number of discovered dynamic features, at a range of target FDR values by
- data-type for each response group. Top and bottom panels represent significant changes at W2 and W14
- 957 relative to baseline respectively. FDR was calculated using the Benjamini-Hochberg procedure.
- 958 Responders were subsampled (n=200) to match the non-responder group size. For responders, mean±
- 959 SEM values are shown.

947

- 960 Supp. Fig 3 | Functional pathways associated with IFX response. a, Scatterplot of p-values obtained by a 961 comparison of pathway scores between W2 and baseline against those obtained by comparing W14 to 962 baseline (-log10 of paired-Wilcoxon P-values shown). Only globally enriched and network connected 963 pathways were included. **b**, Pathway score related dynamics between W2 and W14 relative to baseline. 964 Top 70 pathways are shown. Pathways are ordered by fold change effect size. P-values for pathway score 965 differences between time points were calculated by paired-Wilcoxon test. Significance was determined 966 by FDR<0.05 (Benjamini-Hochberg procedure). c, Heatmap representing a cell-specific contribution for 967 the change in the dynamic pathways. The contribution was determined for each gene in the pathway by 968 regressing its unadjusted fold change expression over the major peripheral cell type frequencies. The 969 reported values represent the mean of the coefficients across all genes in the pathway. d, Correlation of 970 pathway score expression with CRP. All time point and response groups are included. (Spearman's 971 correlation coefficients are shown, P-values are calculated by two tailed probability of the t-statistic, 972 Pathway which significantly correlated with CRP (FDR<0.05, Benjamini-Hochberg procedure) are colored.
- 973 Supp. Fig 4 Comparison of the differential signal between response groups dynamics as obtained by 974 the 'Disruption Networks' framework and standard statistics in the feature level. a, Feature specific 975 differential signal between responders and non-responders dynamics at W2 relative to baseline, based on the top disrupted edge ratio (x axis, FDR<0.1 for dropout significance and 10th top percentile of 976 977 disrupted edge ratio) and standard statistics by Wilcoxon test (y axis, FDR<0.1). b, Scatterplot showing 978 feature specific disruption parameters of mean drop intensity against disrupted edge ratio. Points are 979 colored by quartile thresholds (FDR<0.1 for dropout significance and 10th top percentile of the specific 980 disruption parameter). The feature which agreed with the disruption parameters and standard Wilcoxon 981 test is marked with black border.
- Supp. Fig 5 | Baseline differences of the significantly dynamics disrupted pathways. a, Heatmap representing the feature-level baseline differences among genes in the dynamics meta-disrupted pathway (FDR<0.1, Wilcoxon test). b, Correlation between the canonical cellular frequencies as obtained by CyTOF, and the bulk unadjusted expression of the fiber organization related genes in responders (Spearman's correlation coefficients are shown, P-values are calculated by two tailed probability of the t-statistic). Only significant correlation values are shown (P<0.05 and |r|≥0.5).
- Supp. Fig 6 | scRNA-seq based comparison of the baseline fiber organization related expression between the main cell-types and response groups. The fiber organization scaled score based on its baseline differential genes was compared between PBMCs major cell types, and between response groups for monocytes (Wilcoxon P-values shown).

- 992 Supp. Fig 7 Intermediate monocytes functional pathways associated with the predictive fiber
- 993 **organization signature.** Heatmap representing the top 20 intermediate-monocytes specific enriched
- 994 pathways associated with the predictive fiber-organization related signature is shown. Pathways were
- determined by co-expression network based on the pre-treatment expression of the signature predictive
- genes in intermediate monocyte based on the scRNA-seq data in each response group followed by
- 997 enrichment analysis (Spearman's correlation, thinning net by 0.1 top percentile, P-adjust<0.05 for
- 998 functional enrichment significance by hypergeometric test). Pathways displaying significant differences
- between response groups in each cell subset are colored (FDR<0.05 by Wilcoxon test).

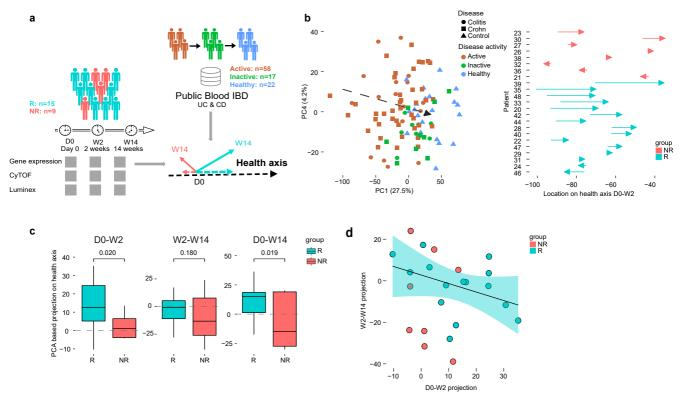
Supplementary Table titles

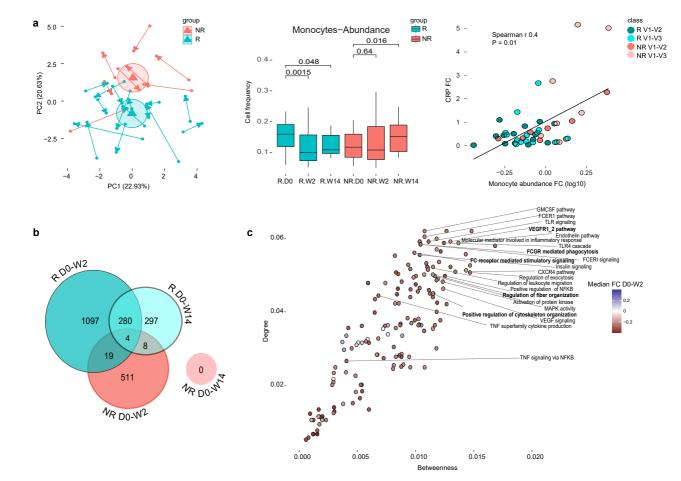
- 1002 **ST1**: Clinical and demographic characteristics of patients included in the primary real life CD cohort
- 1003 ST2: CyTOF Panel

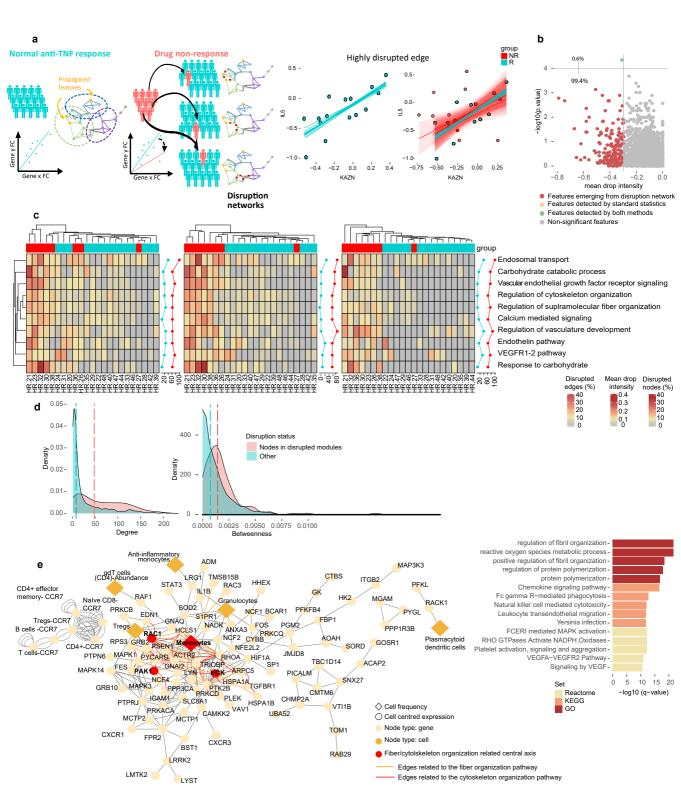
1000

1001

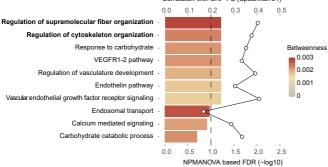
- 1004 **ST3**: Cell type unsupervised clustering using Citrus algorithm
- 1005 **ST4**: Luminex Panel. List of analytes tested in the Luminex assay
- 1006 ST5: Differentially expressed features between CD and UC active patients, and healthy controls for the
- 1007 construction of an external reference 'health axis'
- 1008 **ST6**: Selection of highly informative PCs to best describe an health axis directionality from active,
- through inactive disease states to healthy state using ordinal lasso
- 1010 **ST7**: Dynamic features at W2 and W14 relative to baseline in responders and non-responders using
- 1011 linear mixed-effects models
- 1012 ST8: Normal anti-TNF response dynamics network at the early W2 response period
- 1013 ST9: Clinical and demographic characteristics of patients included in the validation real-life CD cohort
- 1014 ST10: qPCR primers used in the IBD validation cohort for measuring expression of the fiber organization
- 1015 predictive signature

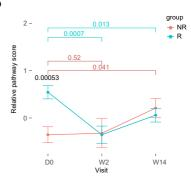


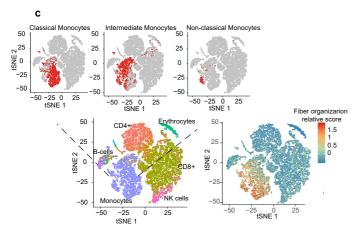


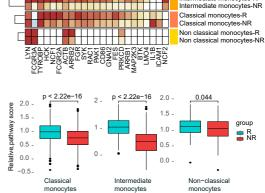












Intermediate monocytes-R

Scaled mean

log2 TP10k+1

d

